DIM-ACAV COLLOQUIUM

Cosmology with weak-lensing peak counts

Chieh-An Lin, Martin Kilbinger

SAp, CEA Saclay

Observatoire de Paris

December 2nd, 2015

This work is supported by grants from Région Île-de-France.

Light deflection

General relativity

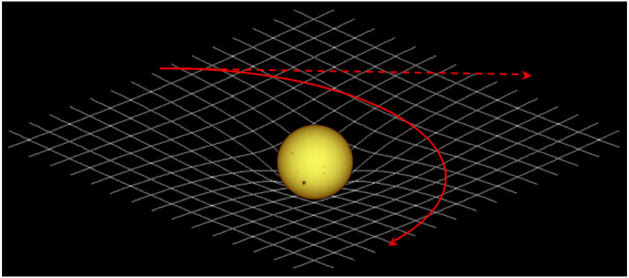

Weak lensing

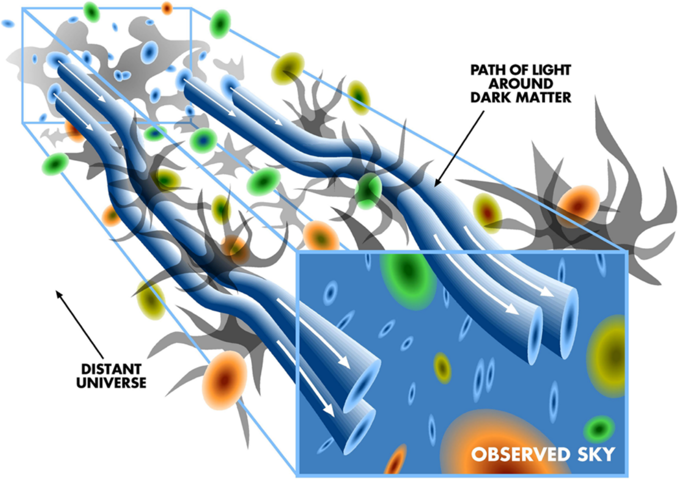

(Source: LSST)

Weak lensing

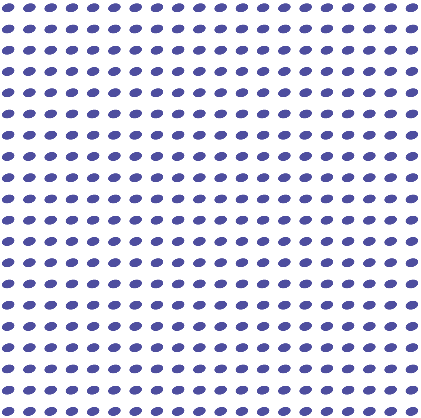

Unlensed sources

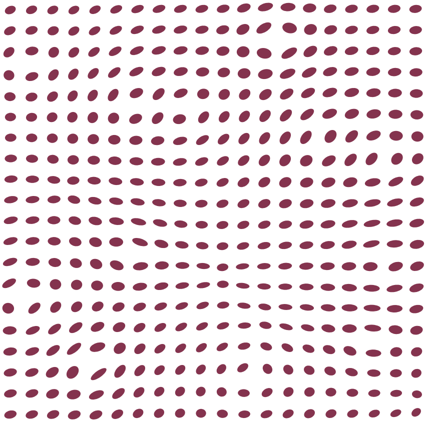

Weak lensing

Lensing formalisms

$$\mathcal{A}(\boldsymbol{\theta}) = \begin{pmatrix} 1-\kappa-\gamma_1 & -\gamma_2 \\ -\gamma_2 & 1-\kappa+\gamma_1 \end{pmatrix}$$

κ: convergence, “projected mass density”

$\gamma = \gamma_1 + \mathrm{i}\gamma_2$: cosmic shear, distortion

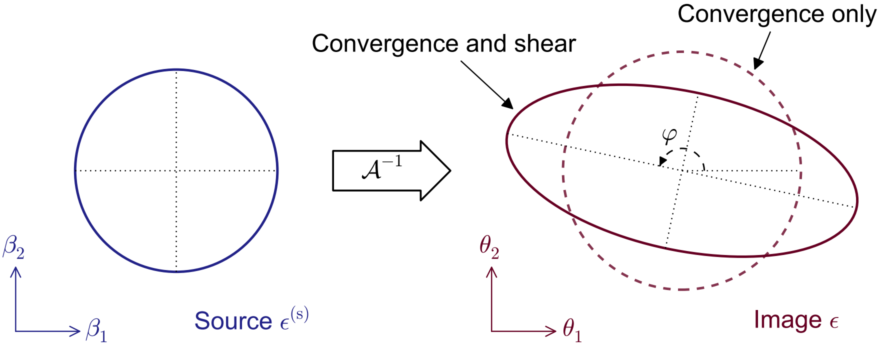

Convergence and shear maps

κ map

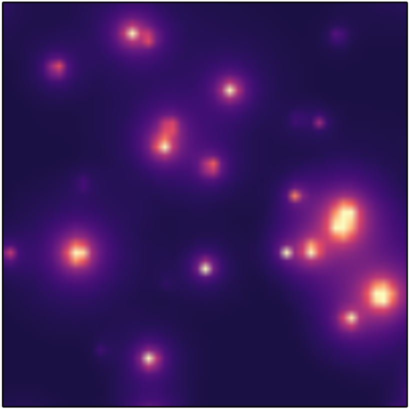

γ map

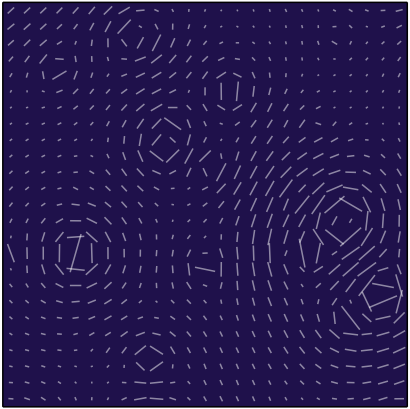

What are peak counts?

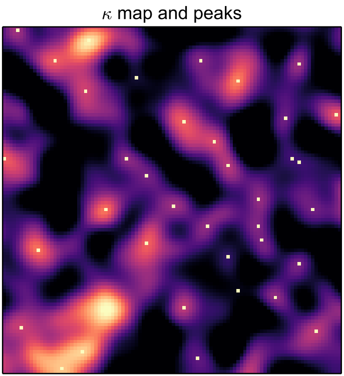

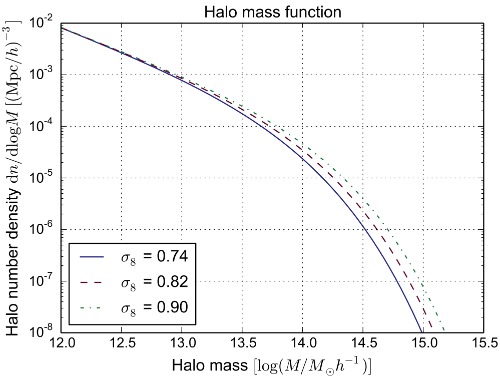

- Local maxima of the projected mass
- Probe the mass function
- Contain non-Gaussian information

Problematic of peak-count modelling

Analytical models for WL peaks

- Maturi et al. (2010) [0907.1849] and Fan et al. (2010) [1006.5121]
- Difficult to handle realistic scenarios: masking, photo-z errors, etc.
- Fail to include additional features: baryons, intrinsic alignment, etc.
- Still require external simulations for covariances

Modelling with N-body simulations

- Very expensive time costs

Challenges

How to model weak-lensing peak counts properly in realistic conditions?

How to extract cosmological information from peaks?

A new model to predict WL peak counts

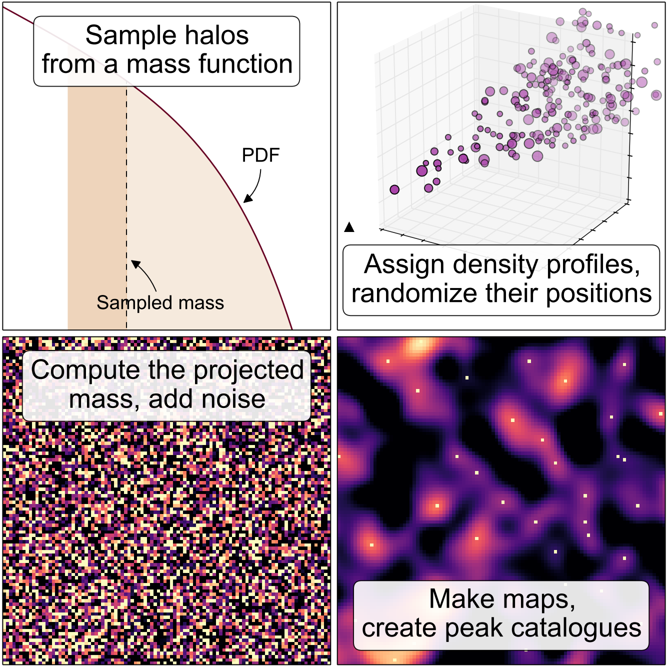

A new model to predict WL peak counts

Hypotheses

- Diffuse, unbound matter does not significantly contribute to peak counts
- Spatial correlation of halos has a minor influence

Public code

CAMELUS

Counts of Amplified Mass Elevations
from Lensing with Ultrafast Simulation

http://www.cosmostat.org/software/camelus/

Advantages

Fast

Flexible

Full PDF information

Advantages

Fast

Only few seconds for creating a 25-deg^2 field, without MPI or GPU programming

Flexible

Full PDF information

Advantages

Fast

Only few seconds for creating a 25-deg^2 field, without MPI or GPU programming

Flexible

Straightforward to include observational effects (e.g. photo-z errors, masks) and additional features (e.g. intrinsic alignment, baryonic effects)

Full PDF information

Advantages

Fast

Only few seconds for creating a 25-deg^2 field, without MPI or GPU programming

Flexible

Straightforward to include observational effects (e.g. photo-z errors, masks) and additional features (e.g. intrinsic alignment, baryonic effects)

Full PDF information

Free from the Gaussian likelihood assumption, allow more flexible constraint methods (copula, varying covariances, p-value evaluation, approximate Bayesian computation, etc.)

Validation

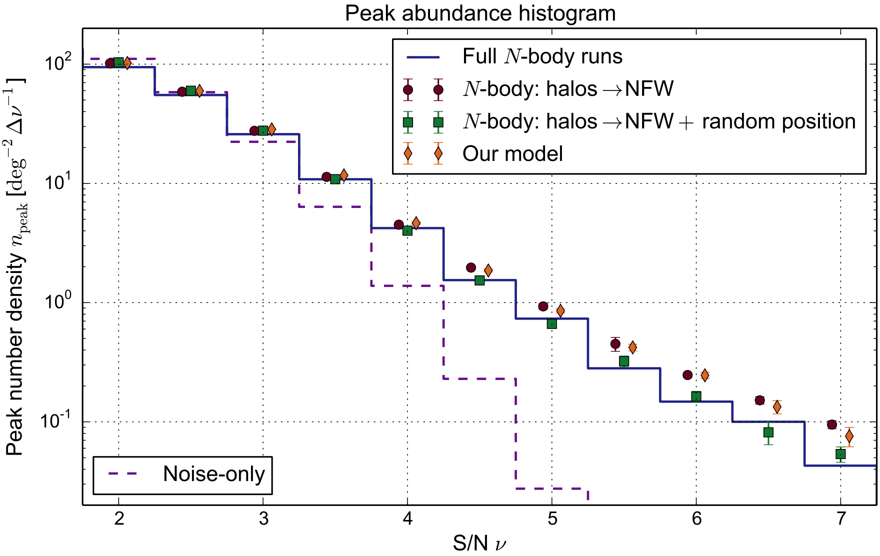

Lin & Kilbinger (2015a)

Cosmology-dependent covariances

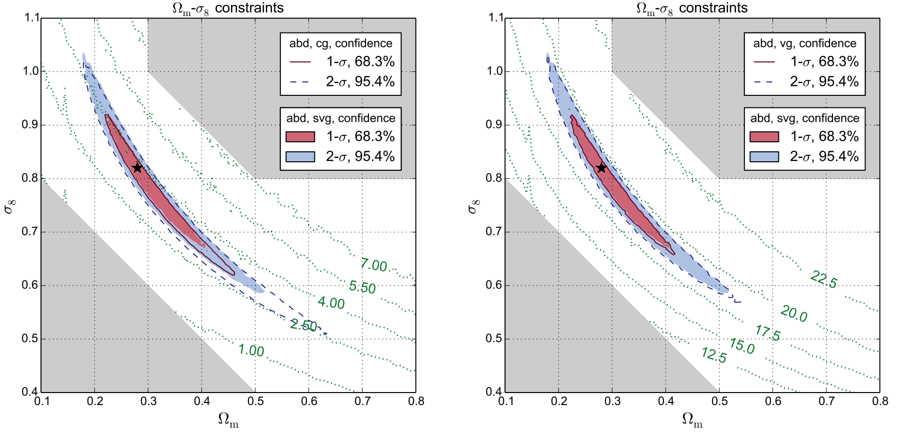

`cg` = constant covariance (lines, left panel)
`svg` = semi-varying covariance (colored zones)
`vg` = varying covariance (lines, right panel)

	cg	svg	vg
FoM	46	57	56

Lin & Kilbinger (2015b)

Approximate Bayesian computation

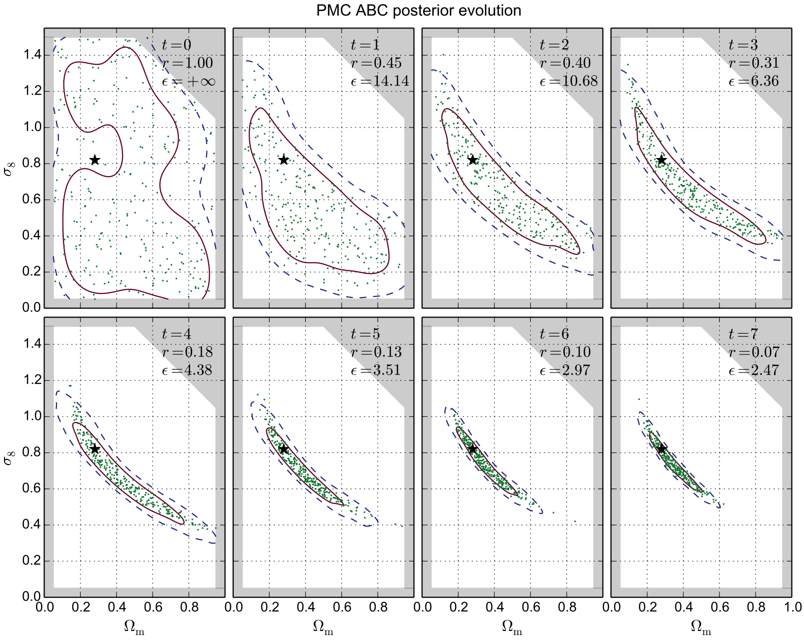

Lin & Kilbinger (2015b)

Approximate Bayesian computation

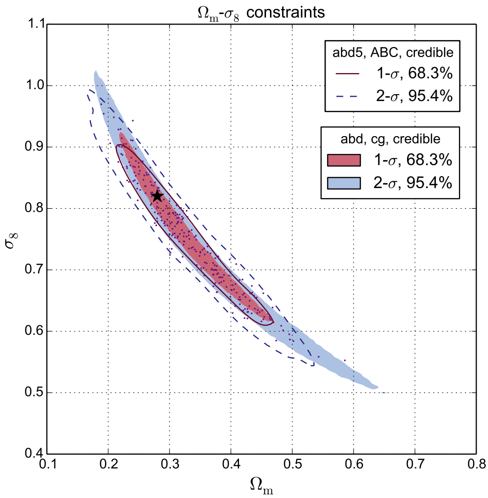

Very good agreement

Time comparison:

- Likelihood $\approx 8000 \times 1000$ simulations to run
- ABC $\approx 250 \times 1 \times 100$ simulations to run

Lin & Kilbinger (2015b)

Perspectives

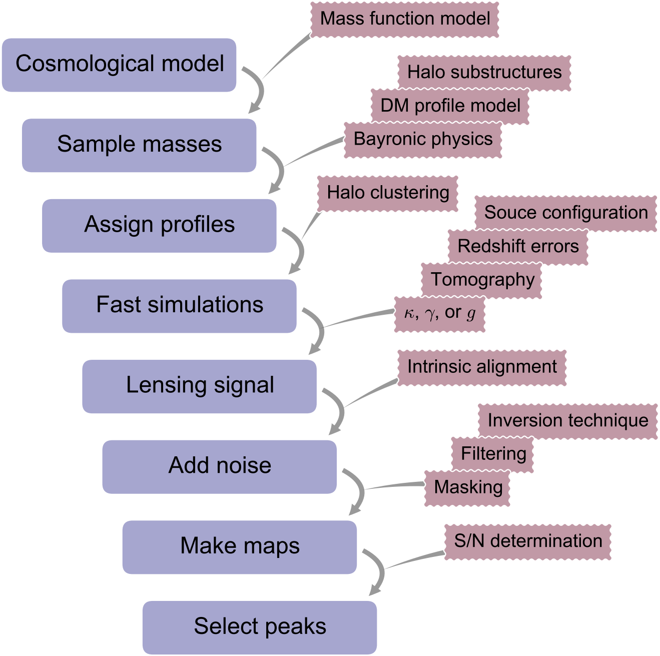

Perspectives

In the framework of this thesis

- Validation of the model (Lin & Kilbinger 2015a)
- Parameter constraint strategies (Lin & Kilbinger 2015b)
- Nonlinear filtering (Lin et al. 2016 in prep.)
- Application to CFHTLenS and KiDS data

Summary

Lin & Kilbinger (2015a,b) — [1410.6955] & [1506.01076]

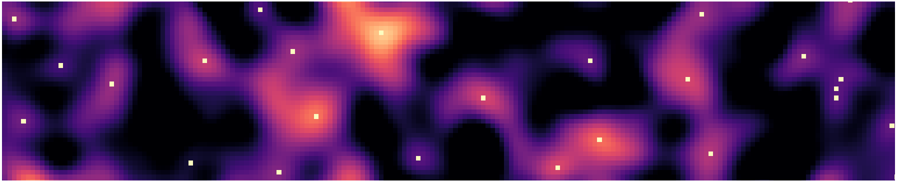

A new model to predict WL peak counts:

Fast, Flexible, Full PDF information

A robust and efficient constraining method:

Approximate Bayesian computation

Backup slides

Born approximation

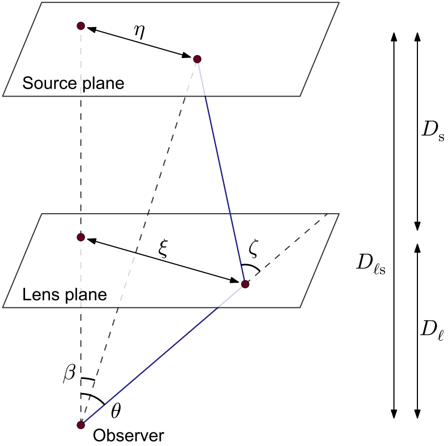

$$\mathcal{A}_{ij}(\boldsymbol{\theta}) = \delta_{ij} - \frac{2}{\mathrm{c}^2} \int_0^w \mathrm{d}w' \, \frac{f_K(w-w')f_K(w')}{f_K(w)} \cdot \phi_{,ij}\left(f_K(w')\boldsymbol{\theta}, w'\right)$$

$$\kappa(\boldsymbol{\theta}, w) = \frac{3H_0^2\Omega_\mathrm{m}}{2\mathrm{c}^2} \int_0^w \mathrm{d}w' \, \frac{f_K(w-w')f_K(w')}{f_K(w)} \cdot \frac{\delta\left(f_K(w')\boldsymbol{\theta}, w'\right)}{a(w')}$$

Settings

- Fixed source redshift z_s = 1.0
- Galaxy number density n_g = 25 arcmin^{-2}
- Pixel size θ_pix = 0.2 arcmin
- Uncorrelated Gaussian shape noise, no IA
- No mask, no baryon
- Gaussian smoothing, with radius θ_G = 1 arcmin

Validation

We compare the following four cases:

- Case 1: full N-body runs
- Case 2: replace N-body halos with NFW profiles with the same mass
- Case 3: randomize angular positions of halos from Case 2
- Case 4: our model

to test our two hypotheses:

- Comparison 1 & 2: contribution of unbound matters & halo asphericity
- Comparison 2 & 3: impact of the spatial correlation
- Comparison 3 & 4: mass function

Low-mass halos seem to be neglgible

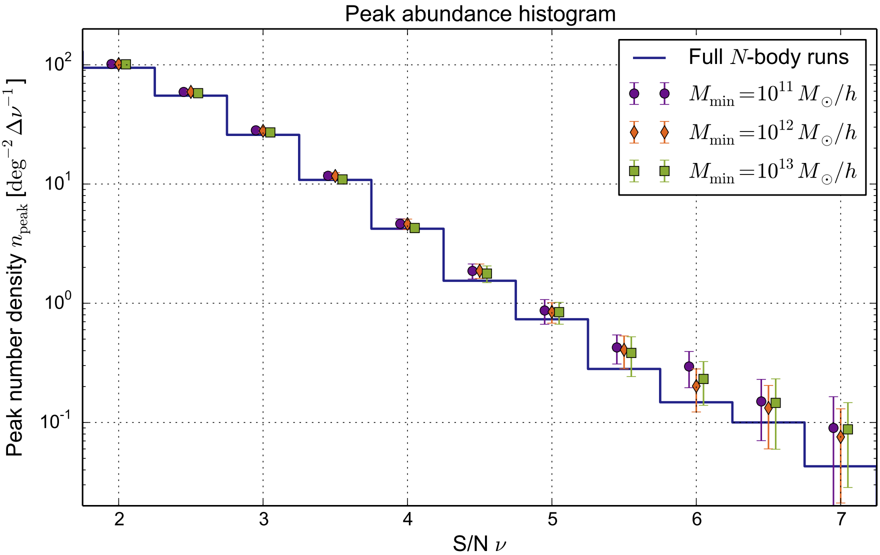

Halo structure parameters should be included in constraints

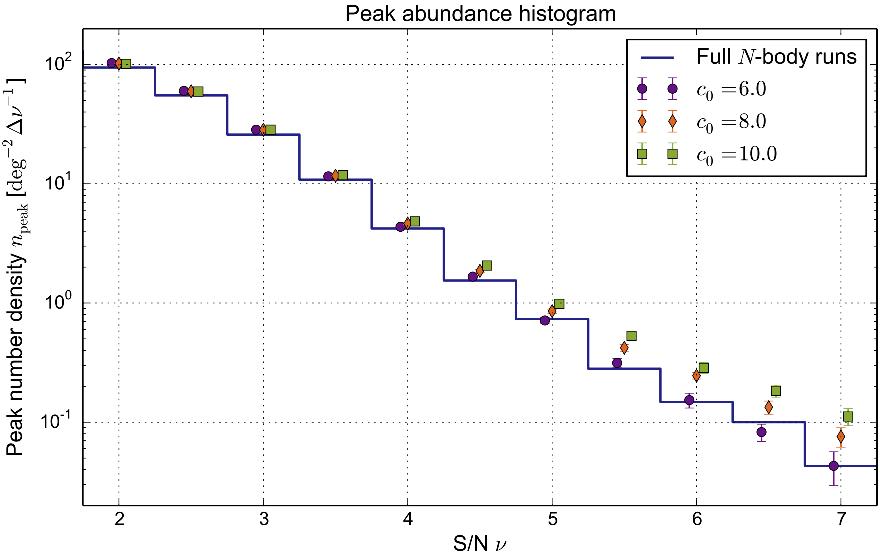

Choice of data vector

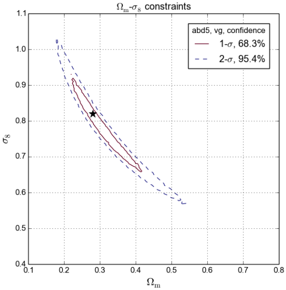

Histogram

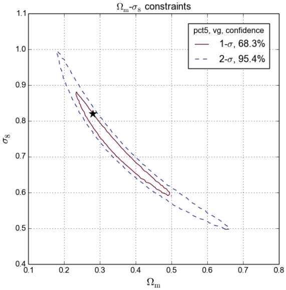

Percentile values

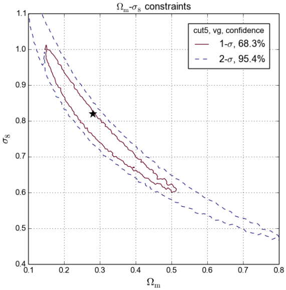

Percentile with cutoff

Lin & Kilbinger (2015b)

Non-parametric methods

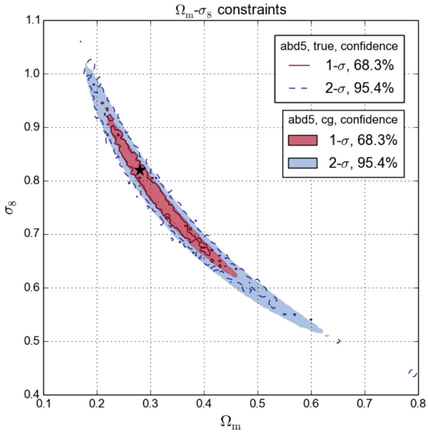

With the true likelihood

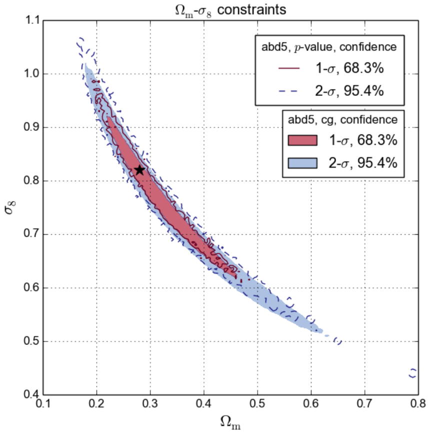

With p-value

Lin & Kilbinger (2015b)

Approximate Bayesian computation

The accept-reject process of ABC samples under $\mathcal{P}_\epsilon(\pi|x^{\mathrm{obs}})$ (red curve),

$$\mathcal{P}_\epsilon(\pi|x^{\mathrm{obs}}) = A_\epsilon(\pi)\mathcal{P}(\pi),$$

where $P(\pi)$ is the prior (blue curve) and

$$A_\epsilon(\pi) \equiv \int \mathrm{d}x \; P(x|\pi)\mathbb{1}_{|x-x^{\mathrm{obs}}|\leq\epsilon}(x),$$

is the accept probability under π (green area).

Meanwhile,

$$\lim_{\epsilon\to 0} A_\epsilon(\pi_0)/\epsilon = P(x^{\mathrm{obs}}|\pi_0) = \mathcal{L}(\pi_0),$$

so $\mathcal{P}_\epsilon$ is proportional to the true posterior when $\epsilon \to 0$.